JOURNAL OF GEOPHYSICAL RESEARCH, VOL. 104, NO. C4, PAGES 7953–7966, APRIL 15, 1999

Settling-driven convection: A mechanism of sedimentation from stratified fluids

David C.J.D. Hoyal
Exxon Production Research, Houston, Texas

Marcus I. Bursik
Department of Geology, State University of New York at Buffalo

Joseph F. Atkinson
Department of Civil Engineering, State University of New York at Buffalo

Abstract. Convection driven by sediment particles may play an important role in sedimentation from the base of buoyant (hypopycnal) plumes, for example, fluvial plumes in stratified estuaries and lakes, black smokers on the ocean floor, volcanic clouds, and coastal currents. In addition to the well-known double-diffusive convection mechanism, another mode of convective instability development is by settling across the density interface. We performed laboratory experiments to investigate this fingering/convective instability mechanism and its effect on particle distribution in the water column and deposition at the bed. A simple theoretical model of finger formation at a fluid density interface is developed based on an analogy with thermal/plume formation at a flat heated plate. This model, which involves a thickening interface layer that becomes gravitationally unstable relative to the ambient fluid, is in good agreement with measurements of finger size and instability wavelength from visualization experiments. Since fingering at the density interface drives larger-scale convection in the fluid below, a mass balance model of the lower layer, assuming strong mixing (i.e., uniform sediment concentration) is successfully applied to predict sediment concentration in the water column and deposition at the bed. Strong mixing can be assumed since convective velocities are usually much greater than the particle fall velocities. As convection proceeds, the sediment concentrations in the two layers approach each other and convection will die out. Using the model equations, we develop analytical expressions for the time when convection ceases and the portion of sediment remaining in the water column.

1. Introduction

Buoyant (hypopycnal) particle-laden flows are a major mechanism of particle transport in numerous natural systems, including fluvial plumes [*Wright*, 1977; *Syvitski et al.*, 1988], currents in the coastal ocean [*Drake*, 1971], black smokers on the ocean floor [*Feely et al.*, 1994], volcanic clouds [*Sparks et al.*, 1991; *Bursik et al.*, 1992; *Carey et al.*, 1996; *Woods et al.*, 1995] and magma chambers [*Huppert and Sparks*, 1984; *Marsh*, 1988]. Models of sedimentation of particles from hypopycnal flows have been developed to understand the morphology of modern and ancient estuarine and lacustrine deposits [*Wright and Coleman*, 1974; *Sturm and Matter*, 1977; *Syvitski et al.*, 1985], as well as suspended particle distribution in the water column in stratified natural and engineered aquatic systems [*Cordoba-Molina et al.*, 1978; *Casamitjana and Schladow*, 1993).

Paper number 1998JC900065.
0148-0227/99/1998JC900065$09.00

When a lighter, well-mixed, suspension of small particles is emplaced above a denser fluid, as in a hypopycnal flow, an instability commonly forms at the density interface, forming fingers and forcing convection in the lower layer. Two major causes of instability development are double diffusion and settling across the interface. In natural marine plumes, transport from the base of the plume may involve a combination of these processes due to the diffusion of heat and salt and the settling of suspended particles. In order to develop useful models of these systems, we must first characterize each process individually and study the end-member processes of double-diffusive convection driven by suspended particles and settling-driven fingering/convection. Some quantitative experimental work has been performed to determine sediment fluxes due to double diffusion [e.g., *Green*, 1987]. However, there has been very little work on the mechanism of settling convection/finger development. Important experimental studies by *Bradley* [1965], *Kuenen* [1968], and *Carey* [1997] suggest that convection may lead to different patterns of sedimentation compared to systems where settling dominates transport in the dense lower layer. However, there is

still a great need to develop models for quantitatively estimating the sedimentation rate by settling-driven convection.

In section 2 we present criteria to ensure that settling dominates double diffusion. The particle flux by double-diffusive convection and the case where double-diffusive convection and settling are of a similar magnitude are the subject of another study [*Hoyal et al., 1999*]. We then present a conceptual model of the settling fingering instability based on an analogy with thermal/plume development at a flat plate [*Townsend*, 1959; *Turner*, 1979, p. 266] and compare it with experimental observations (section 3). Settling-dominated conditions are achieved experimentally by using heavy silicon carbide particles and sugar, which has a low diffusion coefficient, as a density stratification agent. For simplicity, step density stratification is imposed rather than a continuous density gradient. Apart from the characteristics of the fingers, models are also developed for the bulk sediment concentration in the water column and sedimentation rate to the bed (section 4). Experiments to test these model predictions are described in section 5 and compared to the models in section 6. In section 7 we discuss the implications of our models and experimental results to sedimentation from natural plumes and the interpretation of natural plume deposits.

2. Conditions for Settling-Driven Fingering

The physical scenario considered in this paper involves a buoyant suspension of particles emplaced above a denser fluid. This system is originally dynamically stable, and instabilities will develop at the interface over time. Two dominant modes of instability development are double diffusion and settling across the interface. The double-diffusive instability develops due to the differential diffusion of two density-altering fluid properties. As the faster diffusing component diffuses out of the upper layer the slower diffusing substance remains, causing a gravitational instability. Readers may be most familiar with this instability in the context of salt-heat systems where "salt fingers" have been observed in both the laboratory and the ocean. In sediment-laden plumes, double diffusion involves sediment-laden water overlying clearer water below with salt or heat being the faster diffusing substance. As "heat" or "freshness" diffuses out of the base of the plume, the fluid in this region becomes denser than the fluid below, driving fingering which may develop into larger-scale convection.

In contrast, settling convection develops when sediment settles across the interface so that the upper part of the dense lower fluid layer becomes heavier than the fluid below. *Green* [1987] presents a criterion to determine whether double-diffusive convection or settling dominates particle transport across the interface based on the ratio (F) of the flux by double diffusion (F_{dd}) to the flux by settling (F_S):

$$F = \frac{F_{dd}}{F_s} \tag{1}$$

At a density step this criterion might also be used to distinguish whether convection, if it is observed, is due to double-diffusion or settling. For F >> 1 double diffusion dominates the interfacial particle flux, while for F << 1 settling dominates. *Green* [1987] modified the double-diffusive flux presented by *Schmitt* [1979] to accommodate particles rather than a dissolved substance in the upper layer. Assuming conditions at the start of an experiment, that is, the maximum flux with no particles in the lower layer, and no sugar in the upper layer, the double-diffusive convective flux is

$$F_{dd} = \rho b (g\kappa\beta)^{\frac{1}{3}} (\beta C_m)^{\frac{4}{3}} \tag{2}$$

Here b is a nondimensional constant determined by experiment (~1/20), g is the acceleration due to gravity, κ is the diffusion coefficient of the fastest diffusing substance and C_m is the sediment concentration in the upper layer (expressed in units of mass/mass). For a dilute particle suspension the density (ρ) of the uniform upper layer can be expressed as

$$\rho = \rho_f (1 + \beta C_m) \tag{3}$$

where ρ_f is the initial fluid density of the upper layer and β is the volumetric expansion coefficient defined as

$$\beta = \left(\frac{1}{\rho} \frac{\partial \rho}{\partial C_m} \right)_{C=0} \approx \frac{\rho_s - \rho_f}{\rho_s} \tag{4}$$

Here ρ_S is the density of the particles. The sediment concentration defined as mass/mass (C_m) can be converted to concentration in mass/volume (C) by

$$\rho_f C_m = C \left(1 + \frac{C(\rho_s - \rho_f)}{\rho_s \rho_f} \right)^{-1} \cong C \tag{5}$$

The flux by Stokes settling (F_S) is

$$F_s = w_s C \tag{6}$$

where, for small particles,

$$w_s = \frac{g d^2 (\rho_s - \rho_f)}{18 \rho_f \nu} \tag{7}$$

and d is the equivalent particle diameter and ν is the kinematic viscosity of the fluid.

Although in natural systems both double diffusion and settling-driven fingering may be operating at the same time due to the diffusion of heat and salt and the settling of particles, it is our intent in this paper to consider the end-member case of settling fingering/convection. A separate contribution treats the case where double-diffusive convection dominates, as well as those situations in which double-diffusive convection and settling are both important (Hoyal et al., 1999). To ensure that settling dominates the interfacial transport of particles, only experiments with F values less than 0.25 were considered. This was achieved by using heavy silicon carbide particles (specific gravity 3.2) and sugar, which has a relatively low diffusion coefficient ($\kappa \approx 0.5 \times 10^{-5}$ cm^2/s) as the stratifying agent. Specific initial values of F are presented in Table 1.

Another condition for the development of settling fingers is that the suspension behave as a continuum, that is, that if the settling speed of the particles is significantly less than the speed of the fingers (V_f) or

$$\frac{w_s}{V_f} << 1 \tag{8}$$

After they form at the interface layer, initially laminar fingers begin to accelerate and thin as they move downward. A characteristic velocity for the laminar fingers is $B^{2/5}Q^{-1/5}$, where Q is the mass flux and B is the buoyancy flux g'Q. This velocity may also be written $g'^{2/5}Q^{1/5}$. The mass flux (Q) for a finger is the mass of particles settling through the interface at the top of the finger near the interface or $w_S 1/4\pi\delta^2$. Thus, (8) can be written

$$\left(\frac{\pi}{4} \right)^{-\frac{1}{5}} w_s^{\frac{4}{5}} (g'\delta)^{-\frac{2}{5}} << 1 \tag{9}$$

Assuming typical values from our experiments i.e., w_S= 0.00216 cm/s (1000 mesh), C = 0.2 g/L, δ=1 cm, g'=0.13 cm/s^2 , gives a value 0.016 for w_S/V_f, which is much less than 1 as predicted. For the largest particles we used, w_S=0.142 cm/s (280 mesh) at 0.2 g/L, (9) gives 0.49 for w_S/V_f, which is still < 1.

3. Finger Formation and Convection Driven by Settling

To observe the dynamics of finger formation by settling, we performed a number of visualization experiments in a small 15 cm deep tank (12.5 x 12.5 x 15 cm). This tank was equipped with a removable barrier to separate the upper layer of silicon carbide particles and freshwater from the lower well-mixed (uniform density) sugar solution (Figure 4). Photographs of the fingers were taken at different times using a vertical laser light sheet and digital CCD camera. Measurements from these photographs allowed us to observe the dependence of finger diameter, finger spacing (i.e., instability wavelength), and finger velocity on the sediment concentration in the upper and lower layers and on particle fall velocity.

A typical photograph from these experiments is presented in Figure 1. Compared to double diffusive fingers which are usually symmetric in the upward and downward directions (i.e., downward and upward fingers have a similar cross section), settling fingers are asymmetric (i.e., the fingers are much smaller in size than the spaces between them). Settling fingers are also more bulbous and shorter than double-diffusive fingers. They tend to break up just below the interface, entraining ambient fluid and other fingers, to form larger-scale plumes and eventually layer scale convection. Consequently, the ambient concentration in the lower layer remains nearly uniform and much lower than the upper layer due to continual dilution by the lower layer fluid (g' remains high). This mixing was observed to scale with the dimensions of the tanks rather than the fingers. In our various experiments we covered a wide range of F values and noticed a smooth transition from typical double diffusive fingers to typical settling fingers like those shown in Figure 1 [Hoyal et al., 1999].

We will now present a simple conceptual model for the development of settling fingers, which can be compared to measurements from the CCD photographs. Fingering driven by particle settling across a density interface may, in many ways, be analogous to thermal or plume formation at a heated flat plate. This problem has received significant attention because of its relevance to the interaction of the land surface and the atmosphere. In the thermal case a hot fluid layer adjacent to the plate thickens by thermal diffusion and then breaks away as a thermal or plume [*Townsend*, 1959, *Turner*, 1979, p. 266]. Thus for most of the time the process of transfer near the boundary is one of conduction followed by a comparatively short period in which the conditions are locally restored to the original uniform state by the removal of fluid as a plume or thermal [*Howard*, 1964]. The tendency for thermals to form can be quantified in a Rayleigh number

$$\mathrm{Ra} = \frac{g'\delta^3}{k\nu} \tag{10}$$

where k is the thermal diffusion coefficient, δ is a characteristic length scale, and g' is reduced gravity defined as

$$g' = \frac{g\Delta\rho}{\rho_2} \tag{11}$$

It is important to recognize that the length scale commonly used in (10) for the heated plate/thermal problem is the thickness of the thickening boundary layer (see *Howard* [1964] as presented by *Turner* [1979, p. 227]) and not the total depth of the fluid as is often used in Bernard convection. A critical Rayleigh number of 10^3 for the onset of thermals suggested by *Howard* [1964] was in good agreement with experiments of *Townsend* [1959].

Table 1. Summary of Experiments

Mixed or Still	h_1 cm	h_2 cm	Mesh	Particle Diameter, cm	Standard Deviation, cm	$w_{s(1)}$, cm/s	$w_{s(2)}$, cm/s	S_2, g/l	ρ_2, g/cm^3	C_1, g/cm3	F_s, g/cm^{2}s	F_{ds}, g/cm^{2}s	F	t_s, s
Upper														
Still	6	8	400	0.00173	0.0001	0.0320074	0.0318502	30	1.0108075	0.001	3.185E-05	7.49537E-07	0.0235332	
Still	6	8	600	0.00093	0.0001	0.0092496	0.0092042	30	1.0108075	0.0005	4.602E-06	2.97454E-07	0.0646345	
Still	6	8	800	0.00065	0.0001	0.0045184	0.0044962	30	1.0108075	0.0003	1.349E-06	1.50529E-07	0.1115973	
Still	6	8	1000	0.00045	0.00008	0.0021656	0.002155	30	1.0108075	0.0003	6.465E-07	1.50529E-07	0.2328389	
Mixed	6	8	400	0.00173	0.0001	0.0320074	0.0318502	30	1.0108075	0.001	3.185E-05	7.49537E-07	0.0235332	3.5951942
Mixed	6	8	600	0.00093	0.0001	0.0092496	0.0092042	30	1.0108075	0.0005	4.602E-06	2.97454E-07	0.0646345	12.44081
Mixed	6	8	800	0.00065	0.0001	0.0045184	0.0044962	30	1.0108075	0.0003	1.349E-06	1.50529E-07	0.1115973	25.46759
Mixed	6	8	1000	0.00045	0.00008	0.0021656	0.002155	30	1.0108075	0.0003	6.465E-07	1.50529E-07	0.2328389	53.136083
Mixed	32	100	320	0.00292	0.00015	0.0911851	0.0334682	108	1.037109	0.015	0.000502	2.77277E-05	0.055232	9.8006565
Mixed	32	100	280	0.00365	0.00015	0.1424767	0.0522941	108	1.037109	0.015	0.0007844	2.77277E-05	0.0353485	6.2724201

Read 3.19E-5 as 3.19×10^{-5}.

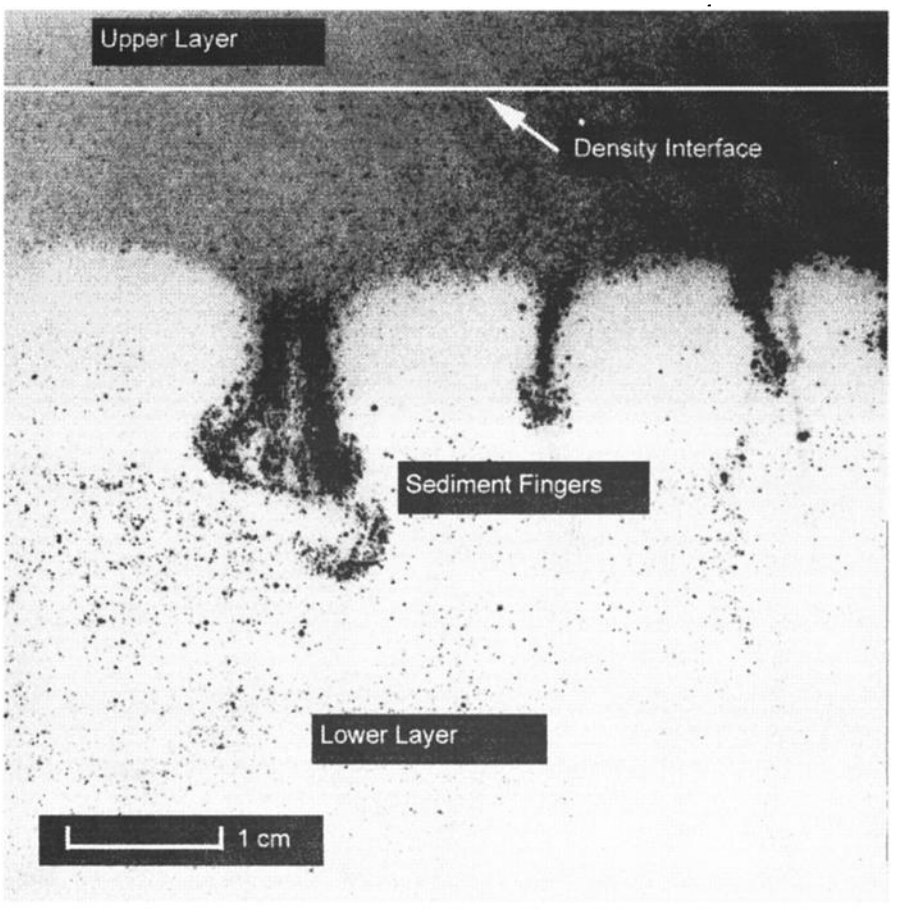

Figure 1. Laser light sheet CCD photograph of settling-driven fingering at a fluid density interface showing the sediment-rich fingers. Suspension is 9.3 μm silicon carbide particles in fresh water overlying an initially clear sugar solution. Note that the area of the fingers is less than the regions of return flow. The instability wavelength (distance between fingers) and the width of the fingers are dependent on the distance of penetration of particles into the lower layer sufficient to initiate convection.

Settling fingers may be analogous in many ways to the above mentioned thermal formation. As the layer of particle-rich fluid (δ) thickens in the lower layer at the settling velocity of the particles w_s, it reaches a critical, unstable thickness and may break off as fingers (Figure 2). In this case the critical conditions might be defined by a Grashof number

$$Gr = \frac{g'\delta^3}{\nu^2} \tag{12}$$

since the Brownian diffusion coefficient of the particles is very low. In analogy to the thermal Rayleigh number discussed above, we assume that δ is the length scale in the Grashof number and that a first estimate of a critical Grashof number (Gr_c) may be 10^3 as in the thermal analog (*Turner*, 1979).

Applying the critical Grashof number definition, we can expect these length scales to scale as a 1/3 power law as a function of g'; that is

$$\delta = \lambda = \phi L = \left(1000\nu^2 / g'\right)^{\frac{1}{3}} \tag{13}$$

Other length scales related to δ include the instability wavelength (λ) (distance between the fingers) and the diameter of the fingers below the interface. Because blobs of fluid that break away are roughly equidimensional, the finger wavelength scales directly with the interface layer thickness ($\lambda \sim \delta$). Since they accelerate as they descend, (not entraining) fingers are thickest near the interface and stretch and thin as they descend. However, their diameter remains proportional to the instability wavelength (size before they break off) so that $\delta \sim \phi L$, where ϕ represents the ratio of the finger at its source to its thinnest point (L). In our experiments it was most convenient to measure the thickness of individual fingers since the lowest-concentration fingers are difficult to observe and so require greater magnification, which makes it difficult to capture two fingers on the same photograph.

To quantitatively test (13), we measured the diameter of a number of fingers (L) for different upper layer concentrations and the same fluid density in the lower layer. All 11 measurements were made at the beginning of the experiment ($\Delta C = C_1$) at the thinnest part of the fingers. Results are presented in Figure 3 as a function of g' with the theoretical power law (13) assuming $Gr_c \sim 10^3$. As expected, the finger diameters very nearly fit a 1/3 power law as a function of g'. The best fit between (13) and our data was achieved using a ϕ value of 5. If our physical interpretation of ϕ as the ratio of the thickness of the base of the finger to the thickness at the thinnest part if the finger is correct, then finger spacing should also be about 5L. This observation was confirmed on our CCD photographs, where we observe that for different values of g', the ratio of finger spacing and finger diameter is a constant of about 5.

Based on this simple conceptual model (13), fingering can always develop if the particle concentration in the upper layer is greater than the lower layer so long as there is sufficient time for

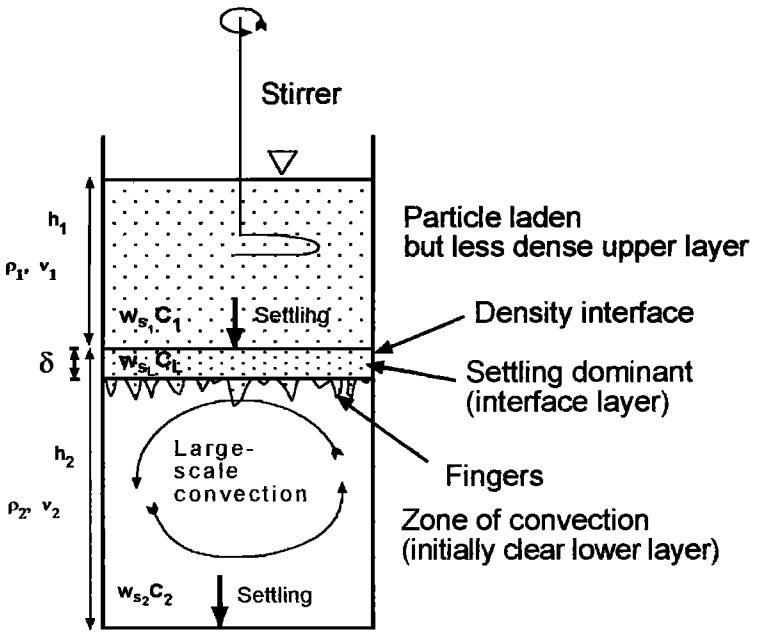

Figure 2. Definition diagram for settling-driven convection. Particles settle out at the base of the upper layer with a flux $w_{S1}C_1$, creating a fingering instability in the lower layer that drives large-scale convection. Sediment settles out at the base of the lower layer by the flux $w_{S2}C_2$. A one-dimensional modeling approach is applied based on the assumption that the lower layer is well mixed. It is assumed that $w_{S1}=w_{S2}$ a reasonable approximation in many flows of interest.

the interface layer to grow to the critical thickness (δ). This settling-driven convection mechanism does not depend on a difference in particle settling speed between the upper and thickening interfacial layer. However, at some interfaces (e.g., air - water) the significant settling speed reduction would increase the particle concentration in the interfacial layer and hence the convection rate [*Carey*, 1997]. At a water-water interface as in our experiments $w_{S1} \sim w_L$; thus $C_1 \sim C_L$ and the only control on g' of the fingers and dependant finger properties is the difference in particle concentration between the interface layer and the lower layer (i.e., C_L-C_2), which is equivalent to C_1-C_2. Observations from our experiments are in agreement with this conceptual model of a thickening interface layer. Predicted layer thicknesses of 0.1-3 cm (equation (13)) are close to those observed experimentally (1-2 cm). The reason that very thin interface layers were not observed in our experiments may be an experimental artifact due to some mixing when removing the barrier between the upper and lower layers.

An important implication of (13) is that finger thickness should evolve over time with ΔC. We may expect that the fingers

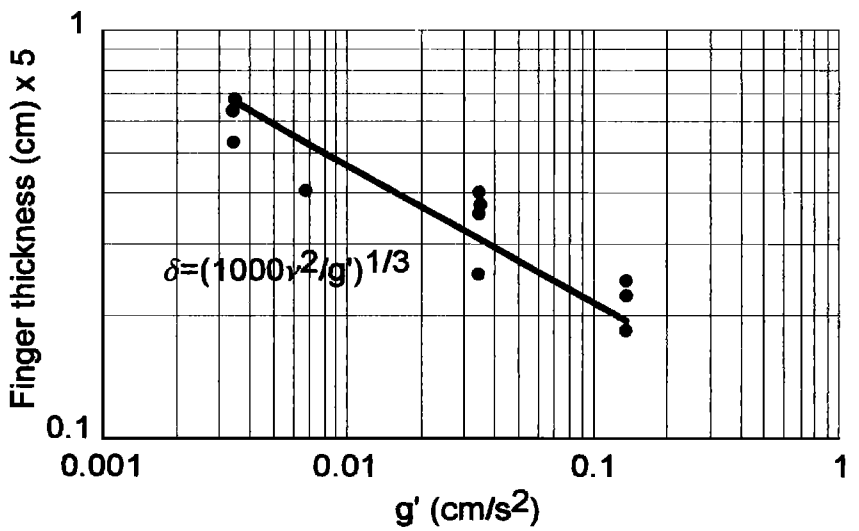

Figure 3. Measured finger thickness at thinnest part (L cm) multiplied by as a function of g' compared with a model based on a critical Grashof number of 1000. Experiments were conducted in small 15cm deep tank (12.5 x 12.5 x 15 cm), lower layer sugar concentration 30 g/L, particle size = 6.5 μm, measurements for upper layer concentrations of 0.005, 0.01, 0.05, 0.02 g/L.

are initially small since the difference between the upper and lower layer concentration is greatest and g' is at a maximum. Over time the particle concentrations in the two layers approach each other, causing an increase in finger diameter and a decrease in the downward velocity of the fingers, both of which are functions of g'. This decrease in velocity and increase in finger size were observed over the course of our experiments. It should be recognized that the analysis described in this section applies to an initial step density profile. If the initial profile in the lower layer is strongly stabilizing the mass of settling particles may not be sufficient for settling convection to develop.

4. Models for Bulk Sedimentation

Having examined some properties of the fingers, we now develop some simple models of vertical sediment transport due to settling fingering/convection. First, we develop models for concentration and particle flux from the upper layer. These models are then applied as input to mass balance models of the lower layer, which predict lower layer concentration and deposition. These models are compared to the experimental results (section 5) in section 6.

4.1. Upper Layer Transport Models

Both strongly mixed and quiescent upper fluid layer were considered, which may correspond to the proximal and distal regions of a plume respectively.

4.1.1. Quiescent upper layer. The loss rate for a uniform mixture of particles from a single quiescent fluid layer with initial concentration C_1 is

$$\frac{dM_1}{dt} = -Aw_sC_1 \tag{14}$$

Here M_1 is the mass of sediment, t is time, and A is the horizontal cross-sectional area of the bed. The fall velocity may be a function of time due to coagulation [*Krone*, 1978; *Kranck*, 1980] or hindered settling [*Barree and Conway*, 1995]. All efforts have been made to reduce coagulation in the experiments, although coagulation effects may need to be taken into account under natural conditions. Hindered settling is not an important effect in the range of low volumetric solids loading encountered in natural hypopycnal flows and used in our experiments. In this study it will generally be assumed that w_S is a constant and that $w_{S(1)} = w_{S(2)}$, which is a reasonable approximation for many of the environmental flows of interest. However, this is not strictly true since $\rho_1 \neq \rho_2$ and $\nu_1 \neq \nu 2$. If $w_{S(1)} \neq w_{S(2)}$ the two-layer models developed below will need to be rewritten to include both settling velocities. Best estimates of $w_{S(1)}$ and $w_{S(2)}$ for our experiments are presented in Table 1. Integration of (14) from 0 to t and substitution with the definition of concentration

$$C_i = \frac{M_1}{Ah_i} \tag{15}$$

(where i=1 in this case) yields the mass of particles leaving the upper layer, or deposited from a one-layer system

$$\frac{M_1(0) - M_1}{M_1(0)} = \frac{w_s t}{h_1} \qquad t < \frac{h_1}{w_s} \tag{16}$$

4.1.2. Turbulent upper layer. A simple turbulent sedimentation model can be developed for a single fluid layer by assuming a uniform distribution of particles with depth . This model, originally developed by *Hazen* [1904], represents the limit of the more general turbulent sedimentation model [e.g., *Dobbins*, 1944] for strong mixing [Cordoba-Molina et al., 1978] and has been successfully applied under a range of natural and experimental conditions [*Krone*, 1978; *Martin and Nokes*, 1988, *Greenberg and Amos*, 1993]. For the case of a uniform concentration of particles mixed continuously, and settling out at the base of the flow, the decay in the mass (M_1) of particles in the fluid column is given by (14). Substitution of (15), solving, and dividing by fluid volume gives

$$C_1(t) = C_1(0)e^{\frac{-w_s}{h_1}t} \tag{17}$$

for the concentration of sediment in the fluid as a function of time (*Martin and Nokes*, 1988). The mass of particles leaving the upper layer, may be determined by integrating the flux (ACw_S) from 0 to t and substituting (15).

$$\frac{M_1(0) - M_1}{M_1(0)} = 1 - e^{\frac{-w_s}{h_1}t} \tag{18}$$

At a fluid-fluid interface, any shear stress powerful enough to resuspend particles would first entrain fluid so that (17) and (18) can only be applied when fluid entrainment is not significant. Field measurements of particle size distribution with distance from a sediment source have confirmed that this model works well in hypopycnal flows in volcanic clouds and estuaries. *Bursik* et al. [1992] applied this model to a deposit from a plinian spreading volcanic cloud in Sao Miguel, Azores. *Bursik* [1995] applied the model to a fluvial plume in a stratified estuary and found good agreement with the data of *Syvitski et al.* [1985, 1988] for Bute Inlet, British Columbia. The model has also been applied with good results to laboratory models of particle-laden plumes [e.g., *Sparks et al.*, 1991; *Ernst et al.*, 1996]. However, precise measurements from laboratory experiments confirming the settling flux across an interface (as opposed to a solid bed) and the robustness of this model have yet to be made, and that is one objective of this study.

If mixed upper layer deepening is significant because of turbulent entrainment, the mass of particles captured (entrained) from the lower layer as well as the effects on h and w_S may need to be taken into account. One approach would be to modify (17) by a probability of deposition as is often done for deposition to a solid bed to account for areas of the bed on which no particles are depositing [*Krone*, 1978; *Greenberg and Amos*, 1993]. This probability should be applied as a coefficient to the exponent in (17) and (18) (i.e., $w_S/h_1 t \rightarrow Pw_S/h_1 t$). An estimate of P for the case where the entrainment velocity (V) is less than w_S is given by

$$P = 1 - \frac{V}{w_s} \tag{19}$$

If $V > w_S$ it may be assumed that no sediment is passing through the density interface. The entrainment velocity is a function of the Richardson number [*Turner*, 1979]. Methods to calculate V for jets or plumes are presented by *Fischer et al.*, [1979].

4.2. Lower Layer Transport Models

4.2.1. Quiescent lower layer. Since it is well known that density stratification reduces significantly the transport of turbulent energy from the upper to the lower fluid layer [*Turner*, 1979], models of sedimentation in estuaries, lakes and volcanic clouds commonly assume that particles are settling individually at their terminal settling speed in the lower dense fluid layer so that a simple settling model, perhaps with some diffusion, has been applied [*Bursik*, 1995; *Casamitjana and Schladow*, 1993]. Settling in the lower layer results in the particles arriving at the bed in the same proportions as it leaves the top layer; that is, the

pattern of sedimentation on the bottom is the same as passes through the density interface with a time delay for the transport of sediment in the lower layer. However, the above discussion suggests that both convective and quiescent transport in the lower layer may occur.

4.2.2. Quiescent upper and lower layer. With quiescent upper and lower layers the loss of mass due to settling from the entire water column, (i.e., $M=M_1 + M_2$) taking into account the time delay for the first arrival of the sediment at the bottom (h_2/w_S), is

$$\frac{M_1(0)-M}{M_1(0)} = \frac{-w_s}{h_1}\left(t-\frac{h_2}{w_s}\right) \qquad t \ge \frac{h_2}{w_s}$$

$$\frac{M_1(0)-M}{M_1(0)} = 0 \qquad t < \frac{h_2}{w_s} \tag{20}$$

4.2.3. Turbulent upper layer, quiescent lower layer. For a fully mixed upper layer and quiescent lower layer the loss of sediment mass is a slight modification of (18):

$$\frac{M_1(0)-M}{M_1(0)} = 1-e^{\frac{-w_s}{h_1}\left(t-\frac{h_2}{w_s}\right)} \qquad t \ge \frac{h_2}{w_s}$$

$$\frac{M_1(0)-M}{M_1(0)} = 0 \qquad t < \frac{h_2}{w_s} \tag{21}$$

4.2.4. Convection in the lower layer. Our laboratory observations indicate that soon after the upper particle-rich layer is emplaced, small fingers form below the interface. However, these small fingers soon coalesce, below the interface into larger descending sediment clouds and then full-blown convection driven by sedimentation from the upper layer. Since the bottom layer appears strongly mixed by convective motions, one approach to modeling convective transport in the lower layer is to assume strong mixing due to convection and apply conservation of mass. As suggested by (9), convective velocities are usually much greater than the particle fall velocity which supports this strongly mixed assumption. The layer may extend to the bottom or not, that is, convection need not necessarily be penetrative. In fact, we performed some experiments with an initially linearly stratified lower layer which show that settling convection will tend to break up a linear stratification into discrete convecting layers, as has been recognized for double-diffusive convection [*Turner*, 1979]. There are basically three phases to a convective sedimentation event: (1) start up (time delay for the first arrival of sediment); (2) strong convection; and 3) cessation of convection (switchover to quiescent water settling). An approximation to the delay time may be calculated by considering the descent time of a non entraining finger or entraining plume using the finger velocity functions presented in Section 2. However, since this startup period is a very small portion of the convection event, our analysis suggests that it can be ignored in many cases.

4.2.5. Quiescent upper layer, convecting lower layer. A mass balance equation for the lower layer can be written

$$\frac{dM_2}{dt} = \dot{M}_{in} - \dot{M}_{out} \tag{22}$$

For a quiescent upper layer, the solution to (22) (bottom layer concentration), assuming $w_{S(1)} = w_{S(2)}$ and $C_2=0$ at t=0, is

$$C_2 = C_1(0)\left(1-e^{-\frac{w_s}{h_2}t}\right) \tag{23}$$

Integrating the flux (CAw_S) between 0 and t and substituting (15), the mass of particles accumulating on the bottom is

$$\frac{M_1(0)-M}{M_1(0)} = \frac{w_s}{h_1}\left(t+\frac{h_2}{w_s}e^{-\frac{w_s}{h_2}t}-\frac{h_2}{w_s}\right) \tag{24}$$

4.2.6. Turbulent upper layer, convecting lower layer. The upper layer is well mixed so that the flux into the bottom layer is w_SA (17) and the lower layer is well mixed by convection so that the mass leaving the bottom layer is C_2w_SA. Assuming $w_{S(1)} = w_{S(2)}$ and $C_2=0$ at t=0, (22) can be solved to give

$$C_2 = \frac{C_1(0)}{1-\frac{h_2}{h_1}}\left(e^{-\frac{w_s}{h_1}t}-e^{-\frac{w_s}{h_2}t}\right) \tag{25}$$

and after integrating the flux (CAw_S between 0 and t), the mass of particles accumulating on the bottom is

$$M_1(0)-M = A\frac{C_1(0)}{\left(1-\frac{h_2}{h_1}\right)}\left(h_2e^{-\frac{w_s}{h_2}t}-h_1e^{-\frac{w_s}{h_1}t}+h_1-h_2\right) \tag{26}$$

or substituting (15)

$$\frac{M_1(0)-M}{M_1(0)} = \frac{1}{h_1-h_2}\left(h_2e^{-\frac{w_s}{h_2}t}-h_1e^{-\frac{w_s}{h_1}t}+h_1-h_2\right) \tag{27}$$

4.3. Criterion for Convection Cessation.

Convection must stop when $C_1=C_2$ and this criterion can be used to estimate a time for convection cessation. Setting (17) equal to (25) and solving for t gives

$$t_c = \frac{\ln\frac{h_2}{h_1}}{w_s\left(\frac{1}{h_1}-\frac{1}{h_2}\right)} \tag{28}$$

These times are presented in Table 1 for the experiments. At t anytime after t_c it may be assumed that particles are settling in a quiescent medium throughout the lower layer. Equation (28) suggests that convection may be short-lived if h_1/h_2 is small. Substitution of t_c from (28) into (27) gives

$$\chi = \frac{h_1-h_2\left(\frac{h_2}{h_1}\right)^{\frac{h_2}{h_1-h_2}}+h_2\left[\left(\frac{h_2}{h_1}\right)^{\frac{h_2}{h_1-h_2}}-1\right]}{h_1-h_2} \tag{29}$$

where χ, is the proportion of sediment deposited (($M_1(0)$-M)/$M_1(0)$) in the convection period t_c. We note that χ is independent of the fall velocity and depends on h_1 and h_2 only. It approaches a maximum of around 0.25 as h_1 and h_2 approach each other. Since in the most optimal case only 1/4 of the particles can deposit during the convection period, this analysis demonstrates that a major role of settling convection is to redistribute particles from the upper to the lower layer, where they may settle by quiescent settling once convection ceases. Equations (28) and (29) are for an upper layer concentration decaying exponentially over time. However, if the upper layer concentration is constant, that is, deposition is defined by (23), the upper and lower layer concentrations approach each other quickly (i.e., exponentially), but theoretically convection never stops since as $t \to \infty$, $C_1 \neq C_2$.

5. Experiments

5.1. Experimental Method

The experiments were carried out in two Perspex tanks, with depths of 15 cm (12.5x12.5x15 cm) and 150 cm (30x30x150

cm). Two fluid layers were set up in the tanks with a lighter suspension of water and particles overlying a denser sugar solution with a sharp interface between them. The use of two tanks enabled us to examine the dependence of the deposition process on the depth of the upper and lower layer suggested in the models. Both tanks had a flexible plastic removable barrier, which ran on tracks glued to the tank walls to separate the two layers prior to the start of the experiment and ensure an initially sharp interface between the two layers. This barrier was removed at the start of the experiments. The large tank was separated into a 102 cm lower layer and a 32 cm upper layer, while the small tank was separated into an 8 cm lower layer and a 6 cm upper layer. A mixture of silicon carbide particles, either 280, 320, 400, 600, 800, or 1000 mesh, and water was then added to the tank and fully mixed prior to removing the barrier. Particle median sizes, standard deviations, and characteristic (median) fall velocities are presented in Table 1. The upper layer of the tank was then either left quiescent or continuously stirred with a rotating impeller driven by an electric motor. In order to reduce particle coagulation, a chemical dispersant (5 g/L sodium hexa metaphosphate) was added to both upper and lower layers and distilled water was used throughout. Sugar, which has a low ionic strength and thus only weakly affects the coagulation of particles, was dissolved in the lower layer to provide a density contrast. The upper and lower layers are initially at the same temperature (20°C), and isothermal conditions are maintained throughout the experiments. Conditions for each experimental run are presented in Table 1.

Sediment concentration in the small-tank experiments was determined by measuring the attenuation of light through the tank at different elevations, allowing detailed measurements of the convection process in time and space, particularly around the interface. The experimental setup is presented in Figure 4. The small tank was set in front of a 15 cm high x 14 cm wide diffuse light source. The light source was set 500 cm from the tank to reduce the chances of heat-driven fluid convection, which was not observed during any of the experiments. On the other side of the tank a vertical array of 12 (3 mm inside diameter) tubes, 15 cm long were mounted horizontally. These received a cone of light that was ~1 cm in diameter on the opposite side of the tank. A vertical array of 12 photodiodes (Burr-Brown, OPT101 integrated photodiode and amplifier) were set behind the tubes to read the light intensity transmitted through the water-particle mixture. The photodiodes were connected to a computer and read every 15 s. Each photodiode was calibrated individually and the light readings converted to particle concentration. Concentration measurement in the deep-tank experiments was achieved by sampling the sediment suspension from taps at different heights and measuring the light attenuation of the samples through a small, flat-sided tube using a digital photographic lightmeter and narrow beam microscope light. Calibrations between light measurements and particle concentration all had correlation coefficients (R) > 0.99.

5.2. Experimental Results

5.2.1. Qualitative description of the experimental results. Detailed vertical concentration-time profiles (surfaces) are presented in Figures 5 and 6 for the small-tank experiments for a quiescent and mixed upper layer respectively. It can be observed that the concentration profiles in the upper layer are quite different. In the unmixed experiment (Figure 5) a slug of sediment with a diffuse upper and lower boundary moves downward over time. In the mixed upper layer experiments the sediment concentration in the upper layer remains uniform but diminishes exponentially over time.

The patterns of sedimentation in the lower layer, however, are remarkably similar. Individual clouds of descending sediment-laden water were not detected; rather, the sediment in the lower layer is almost uniformly distributed from top to bottom due to the great difference between the velocity of the convective motions and the fall velocity of the particles. Typical concentration profiles for the deep-tank experiments with a mixed upper layer (Figure 7) show similar concentration patterns to the small-tank experiments in the lower layer, indicating that this convection process is not restricted to shallow lower layers. In some of the higher-concentration experiments, the convection-driven mixing was strong enough to entrain the top layer into the lower layer and raise the interface. Although the sediment concentrations used in some of the experiments in the large tank were quite high, that is, up to 15 g/L, they are all within the range possible for hypopycnal flows in estuaries.

5.2.2. Results for transport from upper layer. Agreement between the turbulent sedimentation model (equation (17) and the data for the experiments with a well-mixed upper layer is excellent (Figure 8). The theoretically predicted and measured exponential exponents and regression coefficients (R) for the different grain sizes are 400 mesh (-0.24, -0.306, 0.995), 600

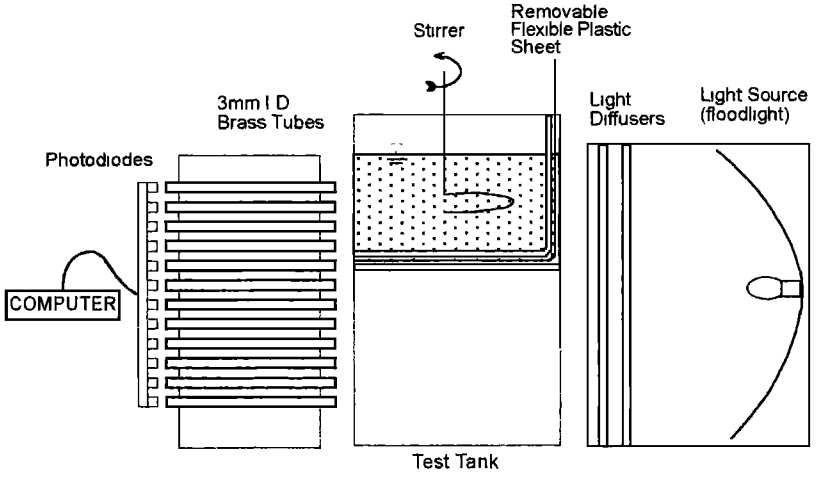

Figure 4. Schematic of the experimental setup (15 cm deep tank)

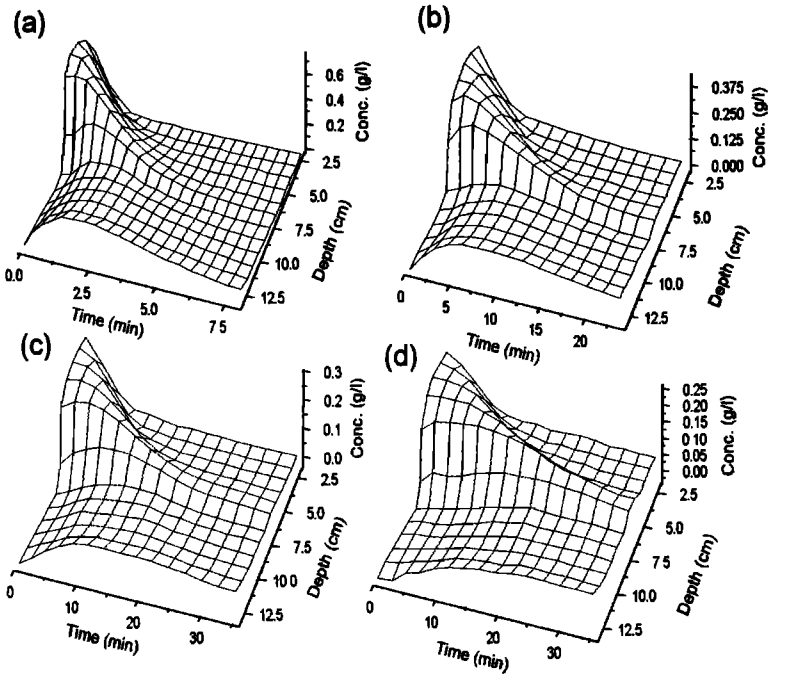

Figure 5. Typical vertical particle concentration profiles as a function of time for experiments with a quiescent upper layer in the small tank of (a) 17.3, (b) 9.3, (c) 6.5, and (d) 4.5 μm silicon carbide powder with a lower layer, of 30 g/L sugar. Data collected every 15 s from 12 photodiodes.

mesh (-0.069, -0.076, 0.998), 800 mesh (-0.034, -0.04281, 0.998), and 1000 mesh (-0.016, -0.01914, 0.995). In all these experiments, fluid entrainment was minimized as much as is possible while still maintaining a uniform distribution of particles with depth. The results suggest that provided fluid entrainment at the interface is minor, this model can be applied to a plume with a uniform distribution of particles or by applying a shape factor, a near-uniform mixture of particles.

The silicon carbide particles used in the experiments were not monodispersed, although their size does have a relatively small standard deviation (see Table 1). These particles were selected because particles with a tighter size distribution were prohibitively expensive in the amounts required for our experiments. Particles in this size range (< 40 μm) are difficult to sieve, but can be separated by sedimentation or elutriation, a very time consuming process [*Fuchs*, 1989].

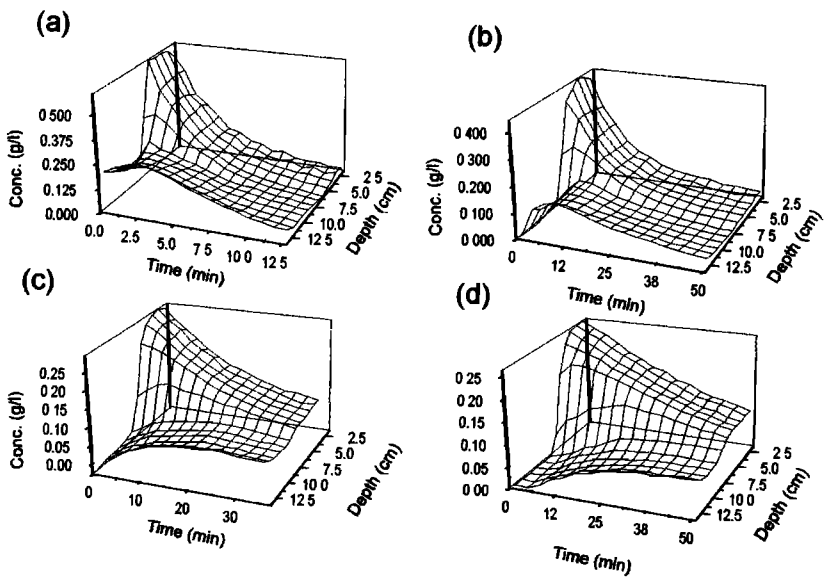

Figure 6. Typical vertical particle concentration profiles as a function of time for experiments with a mixed (turbulent) upper layer, small tank. Depth-concentration-time plots are shown for (a) 17.3, (b) 9.3, (c) 6.5, and (d) 4.5 μm silicon carbide powder with a lower layer of 30g/L sugar solution. Data collected every 15 s from 12 photodiodes.

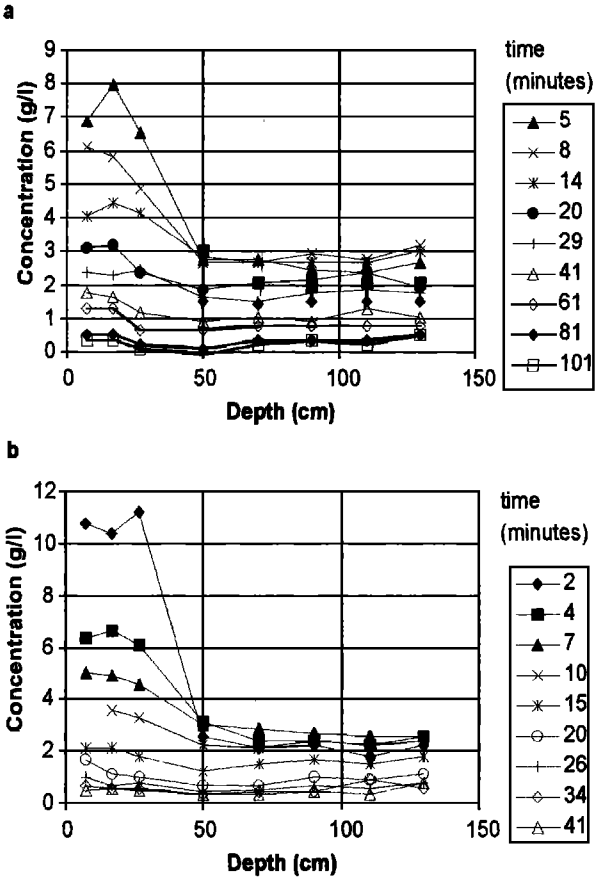

Figure 7. Vertical particle concentration profiles for a mixed upper layer in the deep (150 cm) tank for (a) 29.2 μm, and (b) 36.5 μm silicon carbide particles. The lower layer is 108g/L sugar solution. Symbols denote different time (minutes). The scatter of points in the upper layer for small times (high concentrations) may be an artifact due to the nonlinear calibration curve.

Because our light attenuation-particle concentration calibration curves were based on well-mixed suspensions, there were problems associated with measuring the concentration in quiescent suspensions, which tend to segregate vertically over time. Even weakly polymodal suspensions will quickly separate by gravity and develop a diffuse interface as opposed to the ideal case of a settling unimodal suspension with a sharp upper interface. In addition to this diffuse interface our measurements indicate that the maximum concentration in the upper layer diminished over time. Consequently, the integrated experimental concentrations for the quiescent upper layer experiments compared to (14) did not yield as good a fit as the mixed case. However, if the concentrations were normalized by the maximum concentration at any particular time a much better fit was achieved.

5.2.3. Results for transport in the lower layer. The concentration of suspended sediment in the lower layer of the small tank as a function of time is presented in Figure 9 for a quiescent upper layer and in Figure 10 for a mixed upper layer. Agreement between the models (equations (23) and (25) respectively) and data is generally good, especially for the mixed upper layer. The quiescent upper layer model is only valid in the initial stages because (1) the upper layer is shallow and the initial slug of sediment soon passes through the interface and (2) there are problems of quiescent settling particle size separation as mentioned earlier. Results for the deep box for two particle sizes are presented in Figure 11 and also show very good agreement with the model. These results suggest that simple models based on a well-mixed lower layer provide a reasonable approximation of sedimentation from hypopycnal flows, or at least for our laboratory analogs of real flows.

A slightly better fit between the models and the data could be achieved by taking into account a number of effects. The slight lag in time between the model and experiment for initiation of deposition for the turbulent upper layer experiments with fine particles (Figures 10c and 10d) may have been improved slightly by including a convection startup time as mentioned in section 4.2.4. In the experiments depicted in Figures 10a and 10b the experimental results show a slight time delay which is an experimental artifact due to the finite time it took to set up the experiment, including time to mix the particles initially in the upper layer, remove the barrier, start the mixer, and then start the computer logging. This took approximately 1-2 min, which became significant for the experiments with particles of a higher settling velocity.

5.2.4. Deposition on the bed. The convection models have now been validated, at least for our experimental analogs, by considering the concentration in the lower layer, but how does the deposition of sediment at the bed differ between the traditional models that assume settling in the lower layer and our convective sedimentation models? We present a comparison of the deposition at the bed for different models in Figure 12, calculated for w_S = 0.1 cm/min, h_1=20 m and h_2 = 60 m, which might be representative of some estuarine or volcanic environments. This plot demonstrates that convection in the lower layer has a large effect on the arrival of sediment at the bottom.

The different arrival rates of sediment may also influence the sorting of the bed deposit. To investigate this possibility, we applied the model to different particle size fractions and calculated the distribution of particle sizes with depth in the deposit. In Figure 13 we present the results from modeling the bed deposit for a convecting lower layer and quiescent settling lower layer model. The initial distribution of sediment was lognormal (normal in ϕ) with a mean of 2ϕ and a standard deviation of 7ϕ. We modeled 11 ϕ sizes from this distribution and then numerically determined the properties of the resulting bed deposit. The data are aggregated into two arbitrarily defined layers since most data from natural beds (e.g., varve data, *Sturm and Matter, 1977*) are presented in this way. The difference between the deposits is quite significant. The convecting lower layer deposit has much more overlap (poorer sorting) than the quiescent lower layer. These results suggest that settling driven convection can alter the deposition patterns from a particle suspension and may help explain the sorting of natural beds.

6. Discussion and Conclusions

We have reported here an analysis of convection driven by particle settling at a fluid density interface and laboratory experiments designed to test our analysis. By controlling the suspended particle fall velocity and the stratification agent (sugar), we attempt to minimize double-diffuse effects, which may obscure settling induced convection. Settling fingers do not alter the loss rate from the upper layer, which can be described by a settling flux so long as fluid entrainment at the interface is minimized. However, convection driven by particle settling has a significant effect on the vertical transport of suspended sediment below the plume in the lower fluid layer.

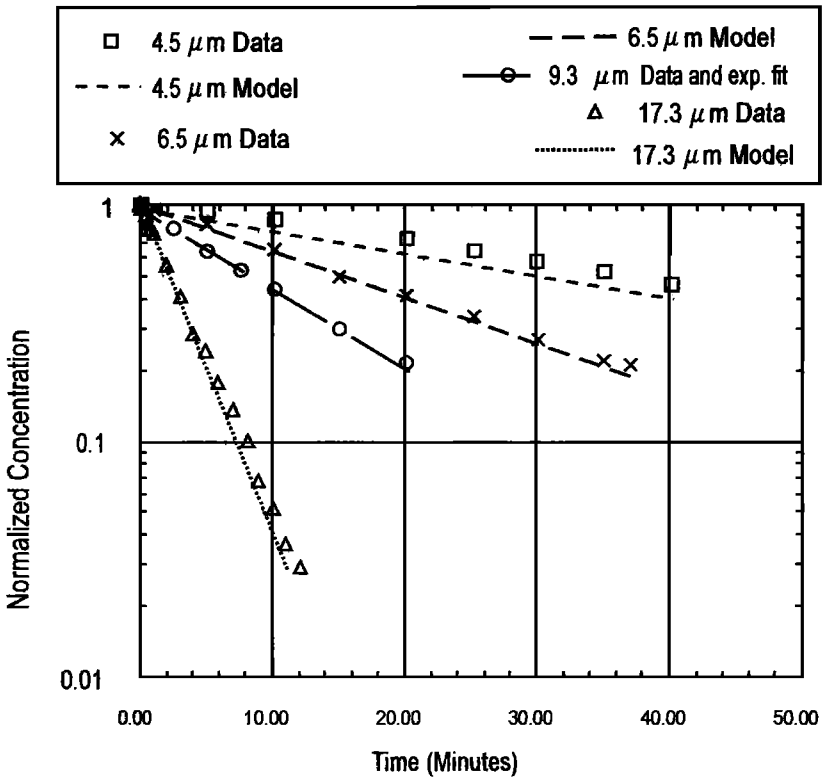

Figure 8. Average concentration in the (mixed) upper layer as a function of time in the 15 cm deep tank for 17.3, 6.5 and 4.5 μm silicon carbide and the model predicted trends (equation (17)). Because of a difficulty reconciling the manufacturer specified and observed settling velocity for the 9.3 μm particles, the model was fitted by least squares regression in this case to obtain w_S for all subsequent calculations.

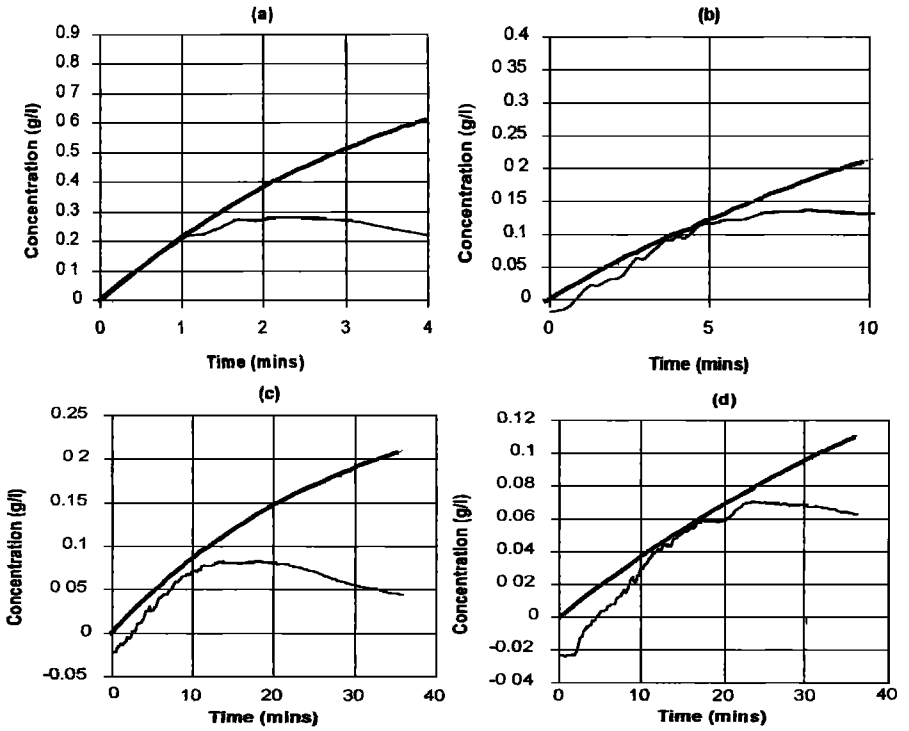

Figure 9. Lower layer concentration as a function of time for a quiescent upper layer in the small box at the 11 cm depth photodiode (i.e., a slice across Figure 5 at 11 cm). Thin line is data and heavy line is the model (Equation (23)). Particle sizes are (a) 17.3, (b) 9.3, (c) 6.5, and (d) 4.5 μm. Concentrations below zero are due to a poor fit of the light-concentration calibration equation at low concentrations. Ideal still water settling predicts a sharp interface moving down so that the model and data should begin to deviate at h_1/w_S. In reality, things are a little different due to the fact that our suspensions are not monodisperse and the settling may drive weak convection, as discussed by *Kuenen*, [1968].

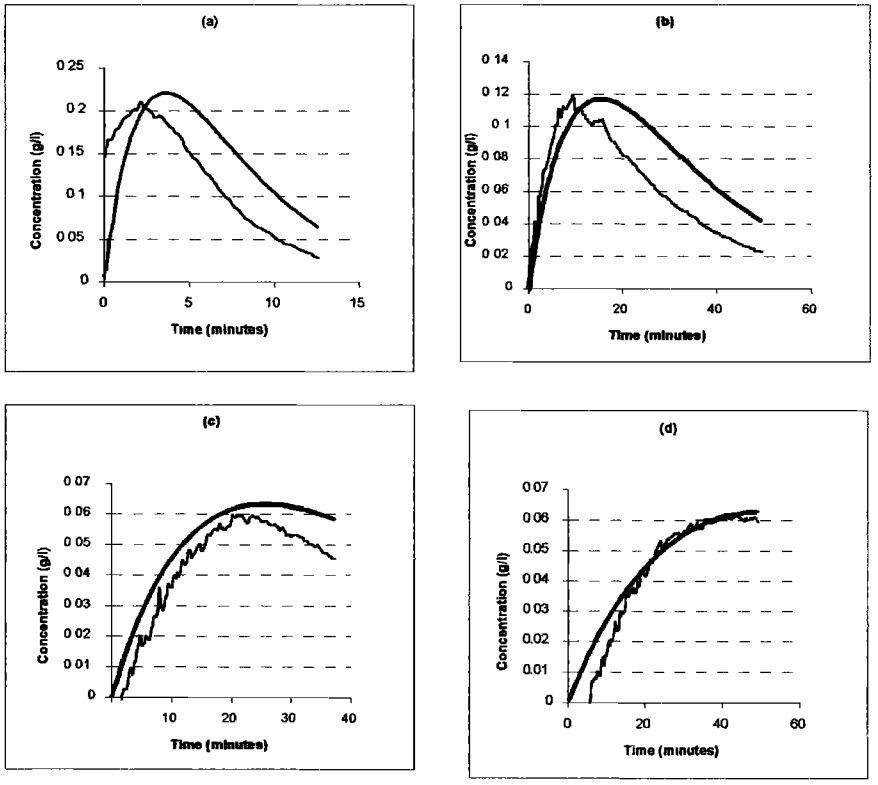

Figure 10. Lower layer concentration as a function of time for mixed (turbulent) upper layer in the small box at the 11 cm depth photodiode (i.e., a slice across Figure 6 at 11 cm). Light line is data and heavy line is the model (equation (25)). Particle sizes are (a) 17.3, (b) 9.3, (c) 6.5, and (d) 4.5 μm.

A conceptual model of fingering/convection driven by settling across a fluid density interface is developed based on an analogy with the production of thermals/plumes at a flat plate. The thickness and spacing of the fingers scale as predicted by this theory. Models developed to describe the vertical sediment concentration distribution in the water column as a function of time are in reasonable agreement with our laboratory experiments. The success of these mixed layer models can be attributed to the much greater magnitude of convective velocities compared to the fall velocity of the particles. The mathematical structure of the models indicates that the ratio of the depth of the upper (h_1) to lower (h_2) fluid layers is a major control on sedimentation patterns.

Step-like vertical concentration profiles observed in our laboratory experiments resemble very closely the sediment concentration profiles in natural particle-laden plumes, suggesting a similar vertical transport mechanism. These patterns differ significantly from the patterns predicted by models based on quies-

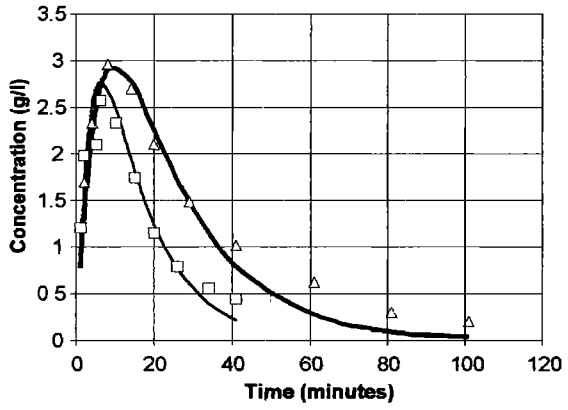

Figure 11. Particle concentration in the bottom layer of the deep tank (C_2) as a function of time. Particles are 36.5 μm (triangles) and 29.2 μm (squares) silicon carbide. Solid lines are model calculations (equation (27)). The upper layer was stirred and samples collected at the second tap from bottom (i.e., 110 cm deep). $S_2(0)$=108 g/L and $C_1(0)$ is 15g/L.

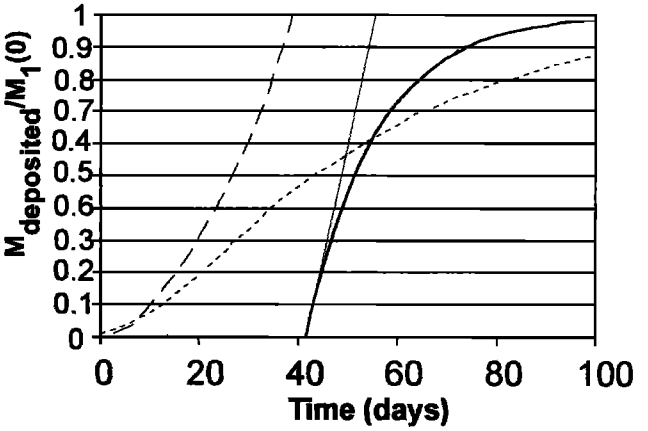

Figure 12. Normalized deposition at the bed [$M_{deposited}/M_1(0)$] as a function of time. The thin solid line denotes quiescent upper layer, quiescent lower layer model (equation (20)). The dashed line denotes quiescent upper layer, convecting lower layer (equation (24)). The dotted line denotes turbulent upper layer, convecting lower layer (equation (27)). The thick solid line denotes turbulent upper layer, quiescent lower layer (equation (21)).

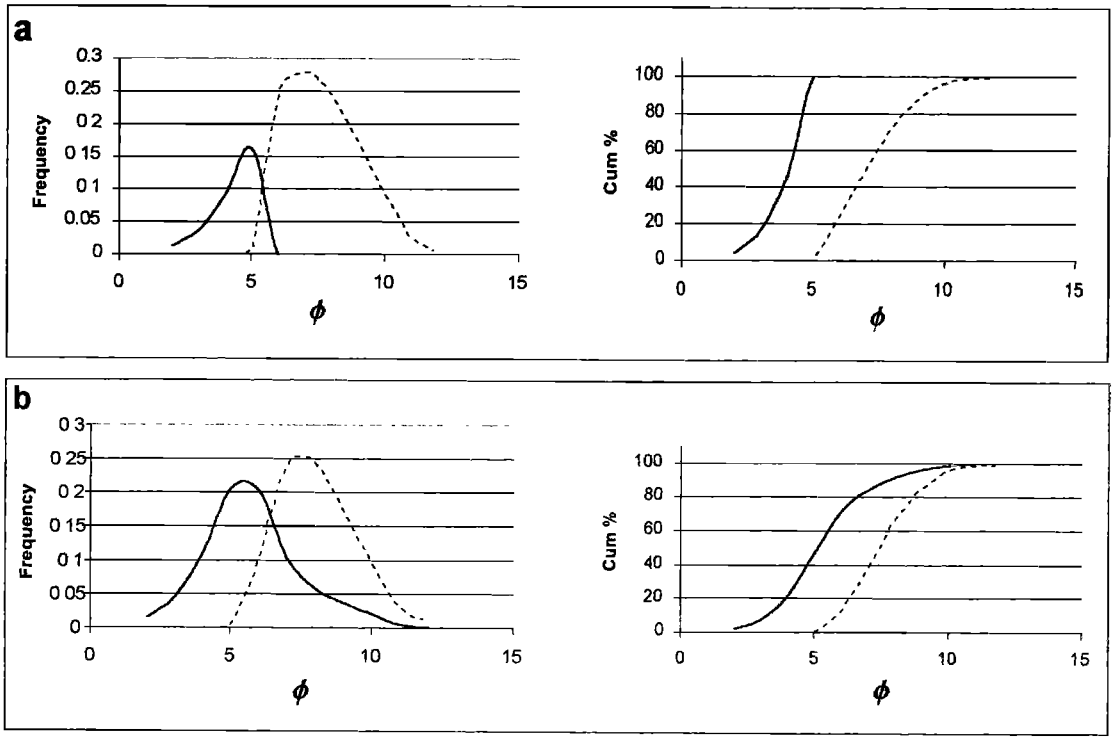

Figure 13. Sorting in the bed deposit for a bed split vertically into two layers, assuming 11 ϕ sizes in the water column distributed according to normal distribution in ϕ with a mean of 2 ϕ and a standard deviation of 7ϕ. Solid line is for upper bed layer, dotted line is for lower bed layer: (a) turbulent upper layer, quiescent lower layer; (b) turbulent upper layer, convecting lower layer.

cent-water settling below the plume [e.g., *Casamitjana and Schladow*, 1993; *Bursik*, 1995]. For example, *Pharo and Carmack* [1979] present data from a well-developed interflow in Kamloops Lake, due to the onset of the spring freshet. They present a vertical slice through the interflow which shows that the base is almost horizontal and coincides with the thermocline while the concentration in the hypolimnion is low and nearly uniform. There is no evidence that settling dominates particle transport below the plume base, which should be indicated by a curtain of turbid water descending at the settling velocity of the particles and perhaps deepening toward the river outlet. A similar picture is evident in the data of *Sturm and Matter* [1977] and *Ford* [1978] presented in *Fischer et al* [1979] (p. 212). Our proposed convection mechanism leads to faster arrival of sediment from the plume at the bed and may affect the sorting of bed deposits. Finger-like protrusions at the base thunderstorm and volcanic clouds may be another example of settling induced convection.

Interesting areas for future research include (1) how does settling convection work in a continuously stratified fluid? (as opposed to a step); (2) what is the effect of horizontal water advection and shear in the lower layer on the fingering and convection?; and (3) is it possible to determine h_1 and h_2 from the sorting signal preserved in the sediments? A treatment of the combined effects of setttling and double-diffusive convection is reported in another study [*Hoyal et al., 1999*].

Notation

β volumetric expansion coefficient for sediment suspension (equation (4)).

χ proportion of sediment deposited when convection ends.

δ interfacial layer thickness.

λ finger instability wavelength.

ρ density of the suspension.

ρ_f fluid density.

ρ_s solid particle density.

κ diffusion coefficient of the fastest diffusing substance.

ν kinematic viscosity.

A horizontal cross-sectional area.

b nondimensional experimentally determined constant.

B buoyancy flux (g'Q).

C_m sediment concentration in mass/mass.

C sediment concentration mass/volume.

C_1 concentration of particles in the upper layer.

C_2 concentration of particles in the lower layer.

C_L concentration of particles in the interfacial layer

d particle diameter.

F flux ratio (equation (1)).

F_{dd} double-diffusive convective flux through the density interface.

F_s flux through the density interface by settling.

g acceleration due to gravity.

g' reduced gravity.

Gr Grashof number.

h_1 depth of the upper layer.

h_2 depth of the lower layer.

h_L depth of the interface layer lying immediately below the density interface.

k Brownian diffusion coefficient of the particles.

L measured diameter of fingers at thinnest part

M_1 mass of particles in the upper layer.

M_2 mass of particles in the lower layer.

P proportion of particles settling through the interface.

Q mass flux.

Ri_c critical Richardson number.
Ra Rayleigh number.
S_1 sugar concentration in the upper layer.
S_2 sugar concentration in the lower layer.
t time.
V_f characteristic velocity of fingers.
W_s terminal fall velocity of a particle (Stokes' law).

Acknowledgments. This research was supported by NSF grant EAR9316656 and by funding from Scientific Applications International Corp. We would like to thank Chen Yu Cheng for help with the models and Alex Eisen for help designing and building the turbidity-measuring device. Andrei Kurbatov assisted with the early experiments.

References

Barree, R.D., and M.W. Conway, Experimental and numerical modeling of convective proppant transport, *J. Pet. Technol.*, 216-222, 1995.

Bradley, W.H., Vertical density currents, *Science*, *150*, 1423-1450, 1965.

Bursik M.I., R.S.J. Sparks, J.S. Gilbert and S.N. Carey, Sedimentation of tephra by volcanic plumes, I, Theory and comparison with a study of Fogo, A plinian deposit, Sao Miguel, (Azores), *Bull. Volcanol.*, *54*, 329-344, 1992.

Bursik, M.I., Theory of sedimentation of suspended particles from fluvial plumes, *Sedimentology*, *42*, 831-838, 1995.

Carey, S., Influence of convective sedimentation on the formation of widespread tephra fall layers in the deep sea, *Geology*, 25(9), 839-842, 1997.

Carey, S., H. Sigurdson, C. Mandeville, and S. Bronto, Pyroclastic flows and surges over water: an example from the 1883 Krakatau eruption, *Bull. Volcan.*, *57*, 493-511, 1996.

Casamitjana X., and G. Schladow, Vertical distribution of particles in a stratified lake, *J. Environ. Eng.*, 119(3) pp. 443-463, 1993.

Cordoba-Molina, J.F., R.R Hudgins and P.L. Silveston, Settling in continuous sedimentation tanks, *J. Environ. Eng.*, *104*, *EE6*, 1262-1275, 1978.

Dobbins, W.E., The effect of turbulence on sedimentation, *Trans. Am. Soc. Civ. Eng.*, *109*, 629-656, 1944.

Drake, D.E., Suspended sediment and thermal stratification in Santa Barbara Channel, California, *Deep Sea Res.*, *18*, 763-769, 1971.

Ernst, G.G.J., R.S.J. Sparks, S.N. Carey, and M.I. Bursik, Sedimentation from turbulent jets and plumes, *J. of Geophys. Res.*, *101*, 5575-5589, 1996.

Feely, R.A., G.J. Massoth, J.H. Trefry, E.T. Baker, A.J. Paulson, and G.T. Lebon, Composition and sedimentation of hydrothermal plume particles from North Cleft Segment, Juan de Fuca Ridge, *J. Geophys. Res.*, *99*, 4985-5006, 1994.

Fuchs, N.A., *The Mechanics of Aerosols*, Dover, New York, 1989.

Fischer, H.B., E.J. List, R.C.Y. Koh, J. Imberger, and N.H. Brooks, *Mixing in Inland and Coastal Waters*, 483pp., Academic, San Diego, Calif., 1979.

Green, T., The importance of double diffusion to the settling of suspended material, *Sedimentology*, *34*, 319-331, 1987.

Greenberg, D.A., and C.L. Amos, Suspended sediment transport and deposition modeling in the Bay of Fundy, Nova Scotia - A region of potential tidal power development, *Can. J Fish. Aquat. Sci.*, *40, suppl. 1*, 20-34, 1993.

Hazen, A., On sedimentation, *Trans. Am. Soc. Civ. Eng.*, 53, 45-88, 1904.

Howard, L.N., Convection at high Rayleigh number, in *Proceedings Eleventh International Congress on Applied Mechanics*, Munich, edited by H. Gortler, pp. 1109-1115, Springer-Verlag, New York, 1964.

Hoyal, D.C.J.D., M.I. Bursik, and J.F. Atkinson, The influence of diffusive convection on sedimentation from buoyant plumes, *Mar. Geol.*, in press, 1999.

Huppert, H.E., and R.S.J. Sparks, Double diffusive convection due to crystalization of magmas, *Ann. Rev. Earth and Planet. Sci.*, *12*, 11-37, 1984.

Kranck, K., Experiments on the significance of flocculation in the settling of fine grained sediment in still water, *Can. J. Earth Sci.*, *17*, 1517-1526, 1980.

Krone, R.B., Aggregation of suspended particles in estuaries, in *Estuarine transport processes*, edited by B. Kjerve, pp. 177-190, Univ. S. C. Press, Columbia, 1978.

Kuenen, PH. H., Settling convection and grain size analysis, *J. Sed. Pet.*, 38(3), 817-831, 1968.

Marsh, B.D., Crystal capture, sorting, and retention in a convecting magma, *Geol. Soc. Am. Bull.*, *100*, 1720-1737, 1988.

Martin D., and R. Nokes, Crystal settling in a vigorously convecting magma chamber, *Nature*, 332(7) 534-536, 1988.

Pharo, C.H., and E.C. Carmack, Sedimentation processes in a short residence intermontane lake, Kamloops Lake, British Columbia, *Sedimentology*, 26, 523-541, 1979.

Schmitt, R.W., Flux measurements on salt fingers at an interface, *Jour. Mar. Res.*, 37, 419-436, 1979.

Sparks, R.S.J., S.N. Carey, and H. Sigurdsson, Sedimentation from gravity currents generated by turbulent plumes, *Sedimentology*, 38, 839-856, 1991.

Sturm M., and Matter, A., Turbidites and varves in Lake Brienz (Switzerland): Deposition of clastic detritus by density currents, in *Modern and Ancient Lake Sediments*, edited by A. Matter and M.E. Tucker, Spec. Pub. No. 2 Int. Assoc. Sedimentol., Blackwell, Cambridge, Mass., 1977.

Syvitski, J.P.M., Asprey K.W., Clattenburg, D.A., and Hodge, G.D., The prodelta environment of a fjord: suspended particle dynamics, *Sedimentology*, 32: 40-65, 1985.

Syvitski J.P.M., J.N. Smith, E.A. Calabrese, and B.P. Boudreau, Basin Sedimentation and the growth of prograding deltas, *J. Geophys. Res.*, *93*, 6895-6908,1988.

Townsend, A.A., Temperature fluctuations over a heated horizontal surface, *J. Fluid Mech.*, 5, 209-241, 1959.

Turner, J.S., *Buoyancy effects in fluids*, Cambridge Univ. Press, New York, 1979.

Woods, A.W., R.E Holasek and S. Self, Wind driven dispersal of volcanic ash plumes and its control on the thermal structure of the plume-top, *Bull. Volcan.*, 57, 283-292, 1995.

Wright, L.D., Sediment transport and deposition at river mouths: A synthesis, *Geol. Soc. of Am. Bull.*, 88, 857-868, 1977.

Wright L.D., and J.M. Coleman, Mississippi River mouth processes: Effluent dynamics and morphologic development, *Jour. Geol.*, 82, 751-778, 1974.

J. F. Atkinson, Department of Civil Engineering, State University of New York at Buffalo, Buffalo, NY, 14260. (email:atkinson@acsu.buffalo.edu)

M. I. Bursik, Department of Geology, State University of New York at Buffalo, Buffalo, NY, 14260. (email:mib@pico.geology.buffalo.edu)

D. C. J. D. Hoyal, Exxon Production Research, P.O. Box 2189, Houston, TX, 77252-2189. (email: david.c.hoyal@exxon .sprint.com)

(Received June 16, 1997; revised July 7, 1998;
accepted September 10, 1998.)